Volume 6 | Number 18 | 21 September 2014 | Pages 7091–7564

Analytical Methods

www.rsc.org/methods

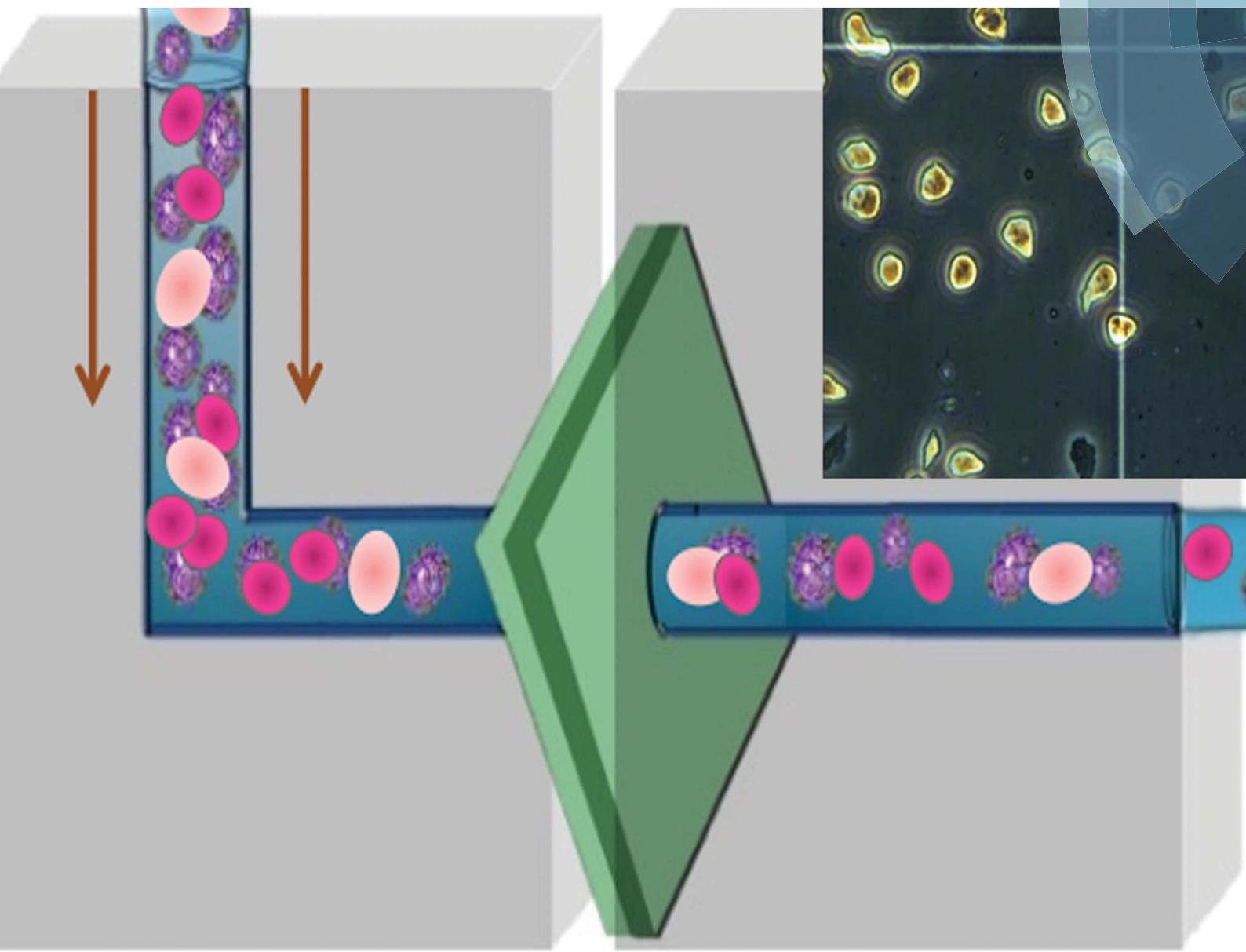

ISSN 1759-9660

ROYAL SOCIETY OF CHEMISTRY

PAPER
Samir M. Iqbal *et al.*
Electrophysiological analysis of biopsy samples using elasticity as an inherent cell marker for cancer detection

Analytical Methods

PAPER

Cite this: *Anal. Methods*, 2014, **6**, 7166

Electrophysiological analysis of biopsy samples using elasticity as an inherent cell marker for cancer detection

Azhar Ilyas,†[abc] Waseem Asghar,‡[abc] Shahina Ahmed,[d] Yair Lotan,[e] Jer-Tsong Hsieh,[e] Young-tae Kim[cd] and Samir M. Iqbal*[abcdef]

Received 30th March 2014
Accepted 27th May 2014

DOI: 10.1039/c4ay00781f

www.rsc.org/methods

Biopsy samples from patients are valuable for diagnosis. Herein, a label-free approach for the early diagnosis of cancer from biopsied samples is reported. The scheme relies on single solid-state micropores as the transducer component and cell elasticity as the indicator of cell health. The biomechanical discrimination of cancerous cells depends on purely intrinsic properties and is not limited by the availability of biomarkers. As a model, bladder cancer cells, which are very different from healthy cells, showed specific electrical signatures. The correlated detection of tumor cells was performed with an efficiency of 75%. The difference in cellular elasticity afforded one order of magnitude lower translocation time for tumor cells. The capability to recognize very few tumor cells solves the prime challenge in biopsy exams. A comparison of the motility and stiffness of cancer and normal urothelial cells showed distinctive quantifiable viscoelastic behavior.

Introduction

Over the last few decades, mortality rates for certain forms of cancer have been the highest. Within contemporary clinical settings, many of the cancers are usually diagnosed at advanced and incurable stages. Common diagnostic approaches vary among cancer types. For example, for bladder cancer, the most common methods include biopsy, cytology, cytoscopy, and the detection of immunological markers. However, these approaches have inadequacies such as flawed judgment (biopsy examination and cytology), high cost (cytoscopy), low sensitivity (cytology and immunological markers) and low specificity (cytoscopy).[1–3] Moreover, the incapability of use at the point of care and the lack of statistical comparison at the single-cell level limit the use of these methods in clinics. Therefore, a more reliable, rapid, and inexpensive detection scheme is critical to diagnose clinically significant but asymptomatic cancers.

Tissue or cell samples taken directly from the area where the tumor is suspected can be the best source to diagnose almost all types of cancers. The procedure used to obtain such samples is called *biopsy*. Open-surgical biopsy or image-guided interventions provide cancer cells of primary tumors from a precise region, but procedural complications present potential risks.[4] Percutaneous biopsy is a typically used clinical procedure that includes fine-needle aspiration (FNA) and core biopsy. FNA employs a very fine needle of 22-gauge (22G) to collect the sample for cytopathology, whereas core biopsy uses a slightly larger needle of 16G or 19G to obtain a small tissue section for histology and immunohistochemical analysis.[5] Percutaneous biopsy has many benefits over open-surgical procedures, including patient compliance, fewer chances of serious complications, low cost and easy processing; however, it involves the risk of missing the suspicious tumor area during biopsy sample collection. Primary and metastatic solid tumors contain cancer cells along with normal cells like endothelial cells, fibroblasts and immune/inflammatory cells.[6] Low-grade cancer and a lack of precision in the case of percutaneous biopsy can lead to a normal cell-enriched sample with too few cancer cells. The conventional testing procedure for such a sample is highly time consuming and technically challenging; thus, the pathologist is more likely to reach erroneous conclusions. This paper presents a simpler and straightforward scheme that is capable of recognizing very few cancerous cells from thousands of normal healthy cells, and it does not require

[a]*Nano-Bio Lab, University of Texas at Arlington, 500 S. Cooper Street, Arlington, Texas, 76019, USA. E-mail: smiqbal@uta.edu; Fax: +1-817-272-7458; Tel: +1-817-272-0228*

[b]*Department of Electrical Engineering, University of Texas at Arlington, Arlington, Texas 76010, USA*

[c]*Nanotechnology Research Center, University of Texas at Arlington, Arlington, Texas 76019, USA*

[d]*Department of Bioengineering, University of Texas at Arlington, Arlington, Texas 76010, USA*

[e]*Department of Urology, University of Texas Southwestern Medical Center at Dallas, Dallas, Texas, 75390, USA*

[f]*Joint Graduate Committee of Biomedical Engineering Program, University of Texas at Arlington, University of Texas Southwestern Medical Center at Dallas, University of Texas at Arlington, Arlington, Texas 76010, USA*

† Current address: Department of Biomedical Sciences, Texas A&M University, Baylor College of Dentistry, Dallas, Texas 75246, USA.

‡ Current address: Department of Computer & Electrical Engineering and Computer Science, Florida Atlantic University, Boca Raton, Florida 33431, USA.

an expert or pathologist and provides statistical comparison based on the behavior of each single cell present in the biopsied sample.

Mechanical properties like elasticity, size, viscosity, deformability, and stiffness of the cells stem from the cytoskeleton, which is an internal polymer network. It defines the shape of a cell, its mechanical strength and important cellular functions.[7,8] Cell division, locomotion and transport of intracellular signals are also tightly coupled with the cytoskeleton.[9] Tumor cells differ from normal cells in various aspects, including morphology, cell growth, cell-to-cell interactions and cytoskeletal organization.[10–13] Changes to cellular functions and morphology of these diseased cells are mirrored in the cytoskeleton.[14] Consequently, the diseased cells exhibit mechanical behaviors, which indicate the physiological status of the cells and can be used as inherent cell markers for the discrimination of cancerous cells.[15]

To date, only a few experimental techniques have been used to study cellular mechanical properties. Micropipette aspiration is one of the prevailing techniques, which applies a negative pressure to the cell and records the aspiration distance as a function of time.[16] Optical deformability, scanning force microscopy, optical tweezers, hydrodynamic stretching, microplate manipulation and acoustic microscopy have also been reported to determine cell rigidity.[14,17–21] All of these techniques have revealed cancerous cells to be softer and less resistant to flow under applied forces. Bladder cancer cells have been reported to be as much as 32 times softer than normal cells using scanning force microscopy.[15] The exceedingly different viscoelastic nature of bladder cancer cells makes them a strong candidate for undertaking elasticity as an inherent cell marker to distinguish tumor cells from healthy ones. Metastatic cancer cells display even higher flexibility, which stems from their need to squeeze through the surrounding tissue matrix to make their way into the circulatory system.[16,22] These discoveries show the possible use of cellular elasticity as a robust cell marker to diagnose the underlying disease. However, all of the present techniques are limited by poor statistical differentiation, low throughput, high cost, need for special preparation, non-physiological handling or cell adhesion due to the mechanical contact of the probe, *etc.*

Solid-state micropores have been used in a variety of sensor applications, *e.g.* electroporation, patch-clamp measurements, measuring the stability of lipid bilayers, monitoring bacterial activities, investigating cell deformability, size-based discrimination, cell counting and measuring electric properties of a single cell.[23–28] Chemical and thermal robustness, mechanical strength and capability to be integrated in a lab-on-a-chip system enable micropores to be used for such diverse studies. Although micropores have been reported for investigating cell deformability or detecting large circulating tumor cells (CTCs) present in the blood, they have never been reported for diagnosing cancerous cells based on merely cell mechanics discrimination between similar-sized cells. Herein, we show single solid-state micropores used as biological transducers that translate cell mechanics into electrical signals. A single micropore on a membrane sandwiched by a dual-compartment setup was used to record the electrical signature of the single cell that translocated through the micropore. The specific pulse characteristics distinguished the cancerous cells from those of the healthy ones and provided a statistical differentiation of each translocated cell in a high throughput fashion. This is a simple and dependable scheme to diagnose bladder cancer. Our device not only evaluates the mechanical properties of cells for correlated detection of cancer cells but also uses behavior of every single cell in the statistical analysis.

Materials and methods

Fabrication of micropore device

All the chemicals were obtained from Sigma-Aldrich (St Louis, MO, USA) unless mentioned otherwise. The fabrication process started with a double-side polished, (100) orientation silicon wafer. After standard RCA cleaning of the wafer, a 200 nm thick oxide layer was thermally grown on it (Fig. 1). Positive photoresist (Shipley S1813) was spin-coated at 4000 rpm for 1 min to obtain a uniformly thick layer of photoresist (~1.2 μm). The photoresist was exposed to UV at a dose of 20 mJ s^{-1} for 7 s and developed for 40 s in MF-319 developer to obtain square windows patterned on one side of the wafer. The other side (bottom side) of the wafer was manually coated with photoresist to shield the oxide from getting etched in subsequent exposure to buffered hydrofluoric (BHF) acid. The square window pattern was transferred to the underlying oxide layer with BHF etching, and then acetone was used to remove the residual photoresist from both sides of the wafer. The wafer was immersed in diluted (25%) tetramethylammonium hydroxide (TMAH) at 90 °C for anisotropic wet-etching of silicon. The silicon wafer was etched (etch rate: 1 μm min^{-1}) through the whole thickness with sidewall angle of 54.7° until an oxide layer on the other side was reached to yield oxide membranes. These thin oxide membranes had wavy topographies, which was due to the internal stresses as shown in Fig. 2(a). A micropore of 20 μm diameter was drilled in each thin oxide membrane using the focused ion beam (FIB) technique. The size of the drilled micropore depended on the FIB milling current, the thickness of the membrane, the material of the membrane and the drilling time.[28–30] The higher the exposure time or the milling current, the larger was the diameter of the resulting micropore. An optimized FIB dose (30 kV acceleration voltage, 1 nA milling current, and 260 second exposure time) was used to drill 20 μm micropores in 200 nm thick oxide membranes. The SEM micrographs of the drilled micropores revealed that the peripheries of the micropores were rough, which could rupture the cell membrane during translocation. Thermal treatment of micropores at 1050 °C for 5 minutes not only helped to make the inner walls of the micropores smoother and flat but also removed the residual stress of the oxide membranes. Fig. 2(b) shows the micrograph of a relaxed and smoothed-out micropore after annealing.

Flow of cells through micropore

The electrophoretic bias alone was not sufficiently strong to make cells translocate through micropores, as is the case in

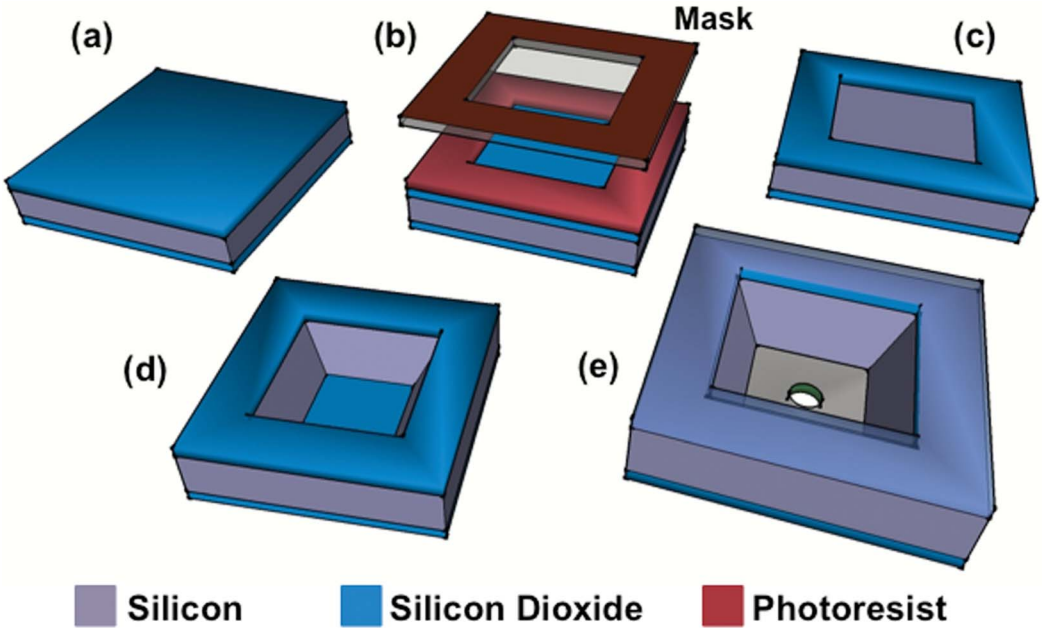

Fig. 1 Process flow for the fabrication of solid-state micropores. (a) Thermal oxidation of double-side polished silicon wafer. (b) Spin-on photoresist, followed by conventional photolithography, to open square windows in resist layers. (c) BHF etching to transfer the square window pattern to the underlying oxide layer. (d) TMAH anisotropic etching of silicon using oxide layer on the other side of the wafer (bottom side) as the etch-stop layer to obtain oxide membrane diaphragms. (e) Drilling of micropore in the oxide membrane using FIB.

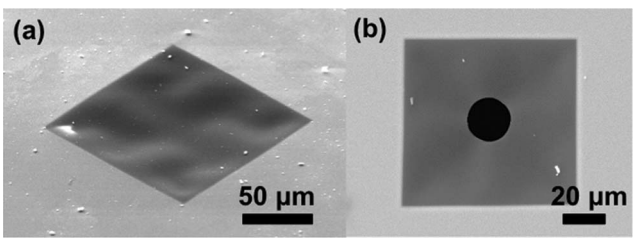

Fig. 2 SEM micrographs of (a) an oxide membrane shows a wavy surface, which is due to the internal stress of the thin film, and (b) a 20 μm micropore after thermal annealing. Note that the membrane is relaxed.

DNA translocation studies with nanopores. Therefore, an optimized fluid pressure was used to push the cells through the micropore. The ionic current flow through the micropore was continuously monitored, and the physical blockage of the micropore resulted in distinctive pulses in the temporal current traces. Pulse magnitude, width and shape indicated the biomechanical properties of the translocated cells and provided the quantifiable viscoelastic behavior of each single cell, which distinctively correlated to the physiological status of the cell.

Experimental setup for electronic fingerprinting of cells

Fig. 3 shows the experimental setup. Two Teflon blocks were used to sandwich the micropore chip. Each block had a small channel ending in a 1 mm opening, which aligned when the blocks were assembled together. The micropore chip was held in place between the two blocks using gaskets made of polydimethylsiloxane (PDMS; Dow Corning). These gaskets restricted leaking of the NaCl solution (0.85% w/v), which was used to fill the compartments. Ag/AgCl electrode pair was used to measure the ionic current flow across the micropore. Data acquisition cards (National Instruments) connected to these electrodes provided voltage biasing and recorded the ionic current. A tubing adapter appended the inlet compartment of the Teflon block assembly to a syringe pump (Harvard Apparatus). The syringe pump injected the cells suspended in NaCl solution into the inlet compartment at an optimal flow rate, while the outlet compartment was filled with NaCl solution only. A polypropylene cell strainer (BD Falcon) with a nylon mesh (100 μm size) was used to obtain a more uniform single-cell suspension and to eliminate any chunks or cell clumps. This was the only pre-processing performed on all the cell samples. When a cell

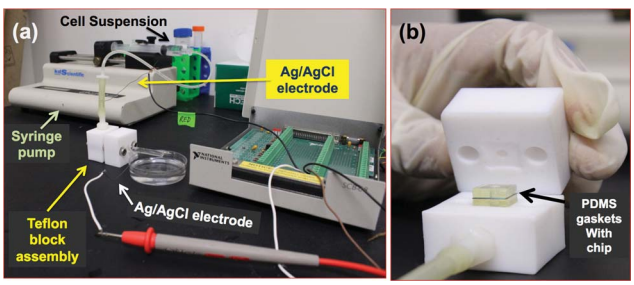

Fig. 3 Experimental setup. (a) Syringe pump pushes the cells to the inlet chamber of Teflon block assembly. The chip with a single micropore is sandwiched between the Teflon blocks. PDMS gaskets are used to avoid leakage, and Ag/AgCl electrodes are inserted in the tubing appended at the inlet and outlet chambers. (b) Inner view of Teflon blocks shows PDMS gaskets sealing the micropore chip.

translocated through the micropore, physical blockage of the micropore offered more resistance to the flow of ionic current. The resistance to the flow of current is given by $R = \rho L/A$, where ρ is the resistivity of the NaCl (0.85% w/v) solution, L represents the thickness of oxide membrane (length of the micropore) and A stands for the effective area of the micropore. Therefore, any variation to the effective area of the micropore due to physical blockage by translocating cells was mirrored in its resistance.

PDMS microchannels to study cell migration

PDMS microchannel devices were fabricated using soft lithography.[31] Each device had 150 μm deep inlet and outlet reservoirs, which were connected through an array of 300 tapered micro-channels (from 20 × 5 μm^2 to 5 × 5 μm^2). Initially, photolithography was conducted to define patterns on a master mold, which was then used to transfer patterns into the PDMS. After punching the fluidic ports, the PDMS device was sterilized, treated with UV ozone plasma for 5 minutes and bonded to a sterilized glass coverslip. Equal numbers of cells (50 000 per device) were seeded in the inlet reservoir and were kept inside the incubator in a controlled environment (37 °C, 5% CO_2 and 95% air) to keep the cells viable. The media was changed periodically, generally within 48 hours. This ensured that there was no nutrient gradient buildup across the channels and amongst the cell types. The cells were allowed to migrate through the microchannels without any chemical gradient or external stimuli. Optical micrographs of migrating cells were captured at regular intervals for up to 4 days (Fig. 4(a)). The number of cells that migrated through the tapered micro-channels and transited to the outlet reservoir during the same length of time were quantified to compare the viscoelastic nature of bladder cancer cells to normal urothelial cells as shown in Fig. 4(b).

Culture of normal human urothelial cells

Immortalized normal human urothelial cells were cultured with T-medium (Invitrogen) supplemented with 5% fetal bovine serum. Cultured normal human urothelial cells appeared as an epithelioid cell monolayer and were enzymatically dissociated with trypsin (0.25%)–EDTA (0.03%) solution for the experiments.

Culture of human bladder cancer cell line

Human bladder cancer cells (T24) were purchased from the American Type Culture Collection (Rockville, MD) and cultured with T-medium supplemented with 5% fetal bovine serum. Once bladder cancer cells were confluent, trypsin (0.25%)–EDTA (0.03%) solution was used to dissociate the cells enzymatically in order to acquire cells for the experiments. Typically, trypan blue assay was used to assess the viability of the cultured cells after trypsinization and >94% cells were found to be healthy.

Results and discussion

All of the trypsinized cells assumed spherical shapes in suspension and were found to be healthy after disaggregation.

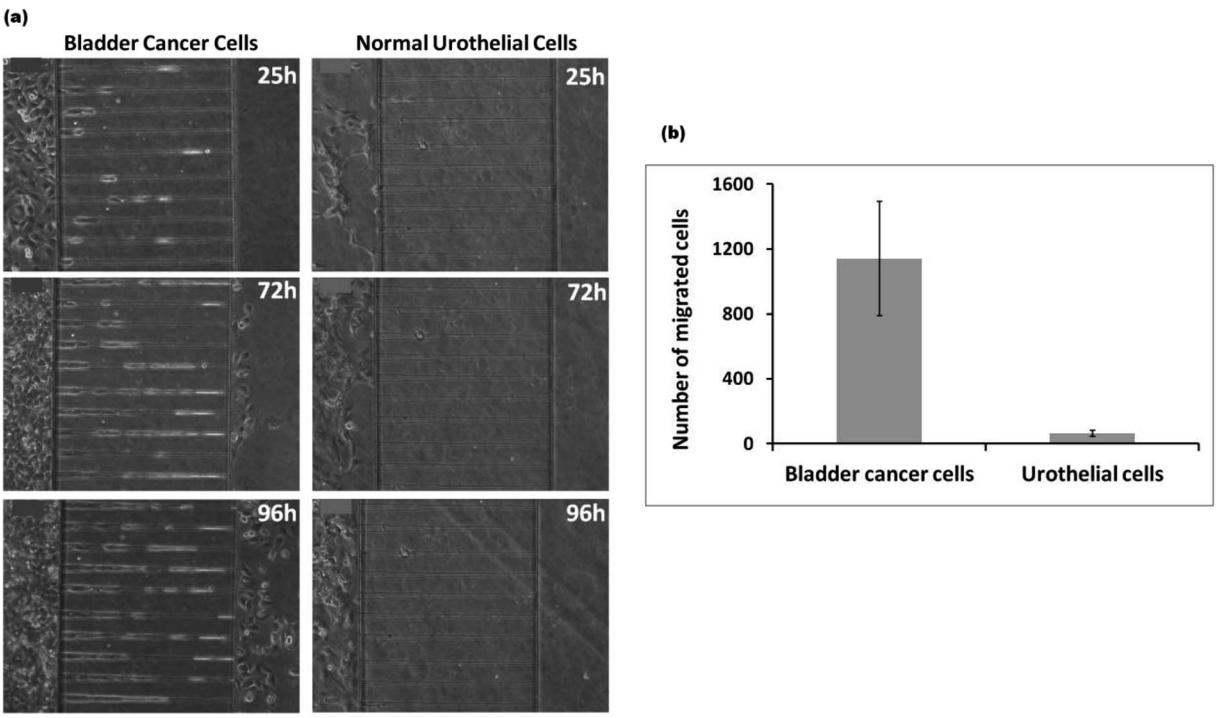

Fig. 4 Comparative study of cell migration through the microchannels. (a) Optical micrographs show that bladder cancer cells are more viscoelastic as compared to normal urothelial cells. The softer nature of bladder cancer cells allows a large number of cells to squeeze and enter the tapered microchannels, whereas the rigidity of normal urothelial cells restrains them from entering into same-sized microchannels over the same length of time (96 hours). (b) Plot demonstrates the quantitative comparison for both types of cells that were able to migrate to an outlet reservoir after 96 hours.

The optical micrographs for both cell types (shown in Fig. 5) demonstrated that bladder cancer cells were nearly equal in size to normal urothelial cells. The average diameter for both cell types was calculated to be in the range of 20–25 μm. This showed that size-based discrimination should be incapable to distinguish between the two types. Fig. 4(a) shows that quite a large number of bladder cancer cells could manage to enter the microchannels. These quickly migrated through the channels and exited to the outlet reservoir during a period of 96 hours. On the other hand, normal human urothelial cells could not even enter the same microchannels in the same time span. This might be due to the flexible cytoskeleton of malignant cells stemming from their faster replication and enhanced motility.[14] There was no chemical gradient across the channel, however, cancer cells could create gradient around themselves (micro-gradient) for several reasons such as fast proliferation and fast consumption of medium as compared to the normal healthy cells. This potential gradient might have initiated the cells' vigorous migration into the tapered microchannels. However, once the cells would reach the confined space (*e.g.*, 8–5 μm width microchannel), they would no longer be able to divide, due to limited space. The cells with capability to dramatically deform their shape vigorously migrated out toward the other side, whereas rigid cells could not migrate through the confined space. We observed approximately 18 times more cancerous cells in the outlet reservoir as compared to normal urothelial cells after 96 hours, which revealed a clear disparity in their morphological flexibility and mobility. Thus, cellular rigidity reflected the physiological status of the cells and showed the power of the presented approach in detecting diseased cells.

A dual-compartment micropore device was assembled as explained in the Materials and methods section. The membrane thickness, micropore size, flow rate and sampling frequency were tuned and tweaked to confine one cell at a time travelling through the micropore and to record the mechanical behavior of each single cell of the sample. A thin silicon dioxide membrane (200 nm) guaranteed single-cell translocation through the micropore at any specific time. Micropores less than 12 μm diameter did not allow the normal urothelial cells to pass through easily and were prone to blockage. On the other hand, micropores larger than 25 μm missed some translocation events; thus, the 20 μm diameter micropore size was selected for its enhanced discrimination without getting blocked. An optimized flow rate of 20 μl per minute was selected to achieve maximum throughput without losing any cell-translocation events. Similarly, the electrical signal sampling frequency was optimized. High sampling frequencies induced a lot of inherent noise, which could suppress some current blockage signals during translocation. Lower frequencies provided a more stable baseline with less noise, but events with translocation times less than the sampling interval could be missed. The optimum ionic current sampling frequency was chosen to be 0.2 MHz, which indicates that electrical signal collection occurred after every 5 μs. A 5 V bias was applied across the micropore, resulting in a 25 mV m^{-1} transmembrane field across the 200 nm long channel. The field would be present only in the area of the membrane and would not build any gradient in the bulk solution.[32] The cell's microenvironment was not affected by this electric field because rapid translocation events were too quick to cause any *in situ* damage to the cells. The cells were examined after translocation through the device and were seen to retain their structural properties and looked similar to unprocessed ones.

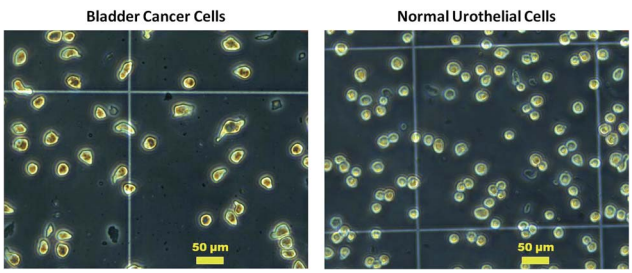

Fig. 5 Optical micrographs showing bladder cancer cells and normal urothelial cells. The cells are spherical in suspension and are observed to be healthy. These images also demonstrate that both types of cells are nearly equal in size (20–25 μm).

Phosphate-buffered saline (PBS) and 0.85 percent NaCl are commonly used physiological solutions for cell suspension.[28,33,34] We suspended the cells in NaCl (0.85% w/v) solution because Ag/AgCl electrodes started losing their AgCl coating in PBS, which was obvious from the whitish ends of electrodes dipped in PBS. The gradual loss of AgCl coating caused an unstable baseline, but the NaCl solution resolved this issue by providing sufficient Cl^- ions for Ag to retain the AgCl coating. The thickness of the oxide membrane defined the area of contact of the cell membrane with the inner walls of the micropore. Micropores of the same size but different membrane thicknesses (200, 330 and 450 nm) were used to study its impact on the translocational behavior of cells. The translocational profile was not significantly affected by varying the thickness of the membrane, but thicker membranes were found to be more prone to blockage/clogging of the micropore (data not shown). Longer channels provided more area for physical contact between translocating cells and the hydrophilic micropore walls, increasing the probability of the hydrophilic phosphate heads of lipid bilayers on cell walls adhering to the micropore walls, which caused plugging of the micropore. Thus, thinner oxide membranes (200 nm) not only ensured single-cell measurement but also removed the possibility of micropore clogging; moreover, they provided sufficient mechanical strength to be used for multiple runs of the experiment.

Different concentrations of bladder cancer cells were used to record the electronic fingerprints of each single cell in the sample. Fig. 6(a) represents the electrical signal trace for a high concentration (20 000 cells per ml) and a very low concentration of cells (100 cells per ml). The frequency of translocation events reflects the cell concentration and can be used for cell counting. The frequency of pulses increases linearly with an increase in the cell concentration regardless of the cell type.[28] The translocation profile was found to be steady throughout the measurements regardless of the cell suspension concentration. Fig. 6(b) shows the electrical signal profile at different time points (1, 10 and 30 minutes) of the recorded data. This showed

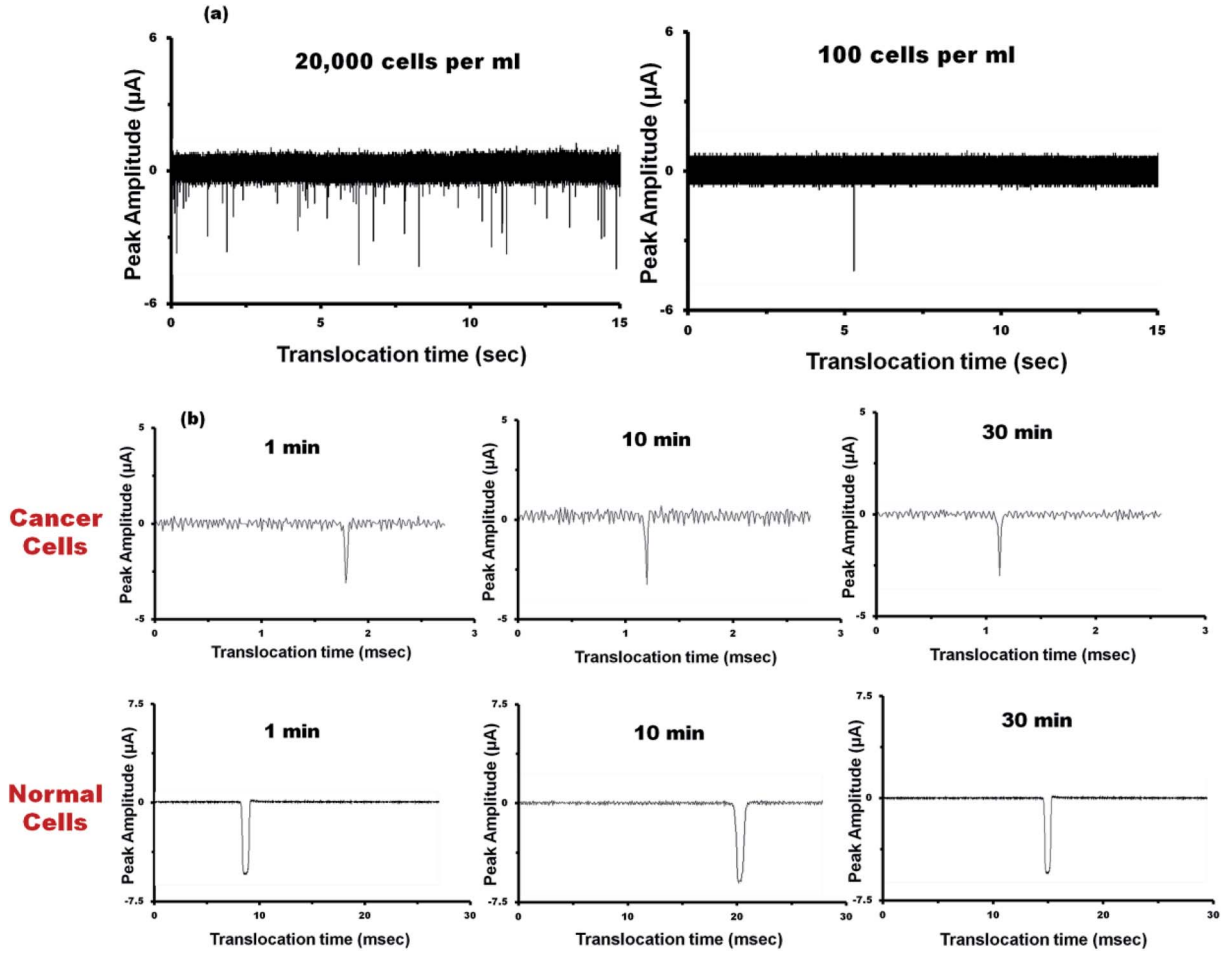

Fig. 6 Cell concentration and reliability. (a) Comparison of the electrical signal for high and low concentrations of cell suspension demonstrates that the frequency of the pulses reflects the concentration of cells. (b) The translocation profile for both cell types remained stable throughout the experiments. The device shows similar current signals at 1, 10 and 30 minutes after initial cell detection for each cell type, which indicates the reliability of the device.

that the micropore stayed open and viable for the measurements.

To distinctively identify and quantify the cells from ionic current fluctuations, the cell suspensions were processed through the micropore. Equal concentrations (20 000 per ml) of bladder cancer cells and normal urothelial cells were suspended in separate solutions, which were processed for 30 minutes in separate runs. The experiments were repeated at least three times, and similar results were observed. The data showed characteristically different translocation profiles for the two types of cell suspensions as shown in Fig. 7(a). The cells provided distinctive current blockage pulses (Fig. 7(b) and (c)). Although a cell strainer was used previously (the only pre-processing step on trypsinized cells) to remove cell clots, a few of the cells were still seen clumped together, which were easily recognized from their current blockage pulse shape as demonstrated in Fig. 7(d). These pulses were discarded from data analysis; thus, only translocation profiles for single cells could be compared. When the cancerous cells passed through the micropore, they were squeezed due to their deformable nature and translocated through the 20 μm micropore in much shorter time compared to their normal counterparts. Rapid translocation events for some of the quickly passing cancerous cells may not have been recorded at the 0.2 MHz sampling frequency, and even if these were measured, their pulse height may have been imprecise. Given the average translocation time of ~8 μs and sampling interval of 5 μs, there is the possibility that some pulses recorded were below the Nyquist limit and were excluded from the analysis. If we added those pulses to the analyses, the data of Fig. 7(a) and 8 would be slightly skewed to the left. Nevertheless, more than 90% of bladder cancer cells were distinctively identifiable from normal urothelial cells by their pulse characteristics (width, amplitude, pulse shape). Although both the cell types were not much different in size, normal urothelial cells showed one order of magnitude increase in translocation time owing to their stiffer nature.

The pulse shape can explicitly describe the orientation of the translocating entity.[28,35] The ionic current through the micropore corresponded to a cross-sectional circular contour, which portrayed the particular physical dimension of the confined

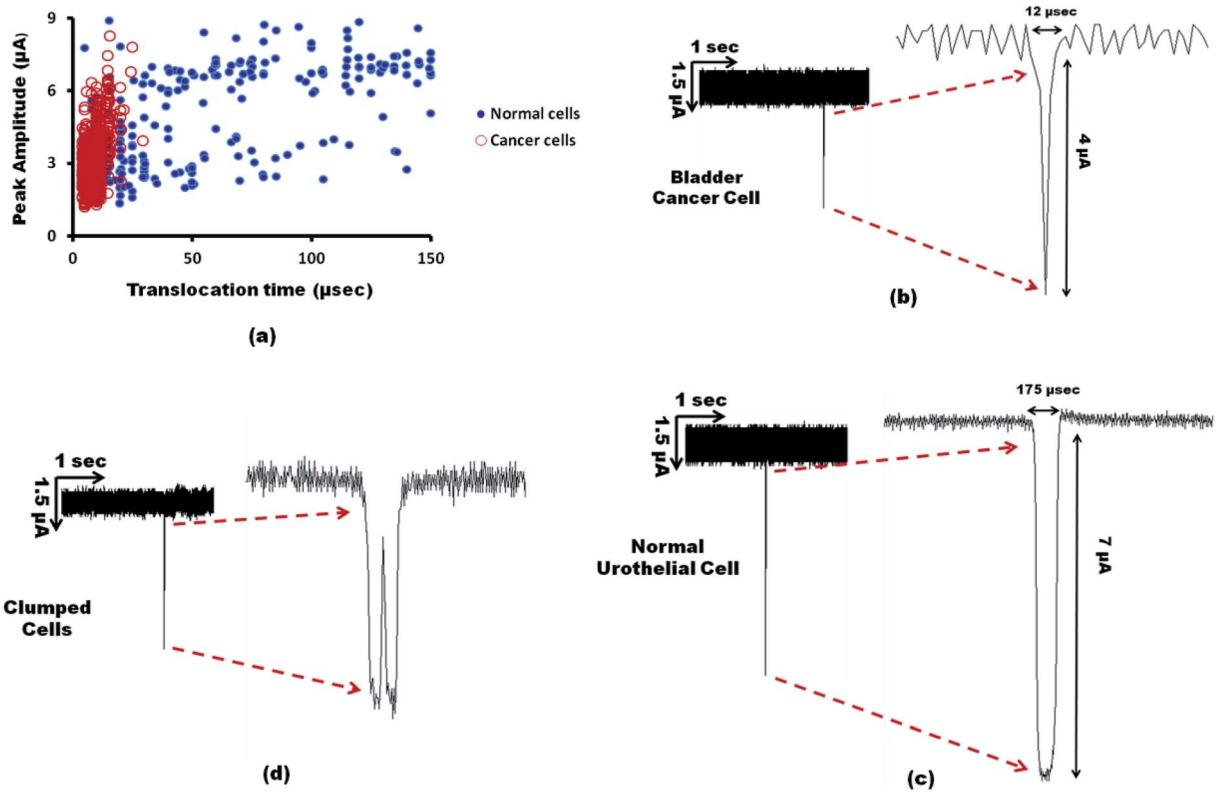

Fig. 7 Scatter plot and translocation profile of the cells passing through the micropore. (a) The distribution of pulses for both types of cells processed separately through the micropore device is shown on a single plot for comparison. The plot indicates that cancer cells show distinctively different electrical profiles when compared to their normal counterpart. (b) and (c) demonstrate characteristic translocation current traces (translocation time, current peak amplitude) for bladder cancer cells and normal urothelial cells, respectively. (d) The pulse shape clearly shows that the signal is from the clumped-together cells. This information is used to eliminate these data points from the analysis.

cell. The outline of the translocated cell predominately defined the pulse shape, whereas the cell's biomechanical properties characterized its translocation profile. The pulse statistics (average translocation time and peak amplitude) for the two cell types are shown in Table 1. The average values were calculated based on thousands of pulse signals for each particular cell type. The reproducibility of the data was verified by repeating the experiments at least three times by using different micropores of the same size, and similar results were observed when processed at optimized conditions. Statistical analysis based on translocation time and peak amplitude was performed using one-way ANOVA for independent samples, and it demonstrated that the two types were significantly different from each other (p-value < 0.001).

Again, although statistical analysis showed that the two cell types were significantly different in terms of their transit times, as well as peak amplitudes, the discrimination of cancerous cells was more related to distinction in translocation time (one order of magnitude difference) than the peak amplitude. Therefore, the detection efficiency of the system was not notably affected by the artifacts resulting from peak amplitude recorded for pulses that were below the Nyquist limit, which would slightly skew the data towards the lower peak amplitude side. The higher sampling frequency could provide more accurate peak amplitudes for faster events, but it would increase the background noise affecting the sensitivity of the device by suppressing the smaller current blockage signals (in the range of 1–2 μs). Thus, here lies the old question of sensitivity *versus* selectivity. The sampling frequency of 0.2 MHz was optimized with all other experimental process parameters to have a high sensitivity of about 92% and a detection efficiency of 75%.

The normal human urothelial cells showed a greater spread of data because the plugging effect of the stiffer cells gave jolted and fluctuated pulses. The micropore not only discriminated the cancerous cells but also provided adequate information to exactly trail the 3D profile of the translocated cell.

After defining the pulse characteristics (pulse duration, peak amplitude, pulse shape) for each cell type, the bladder cancer cells were mixed with normal urothelial cells at different concentration ratios (1 : 1, 1 : 10, 1 : 100, 1 : 1000) to detect the presence of cancerous cells in the mixture. The data was recorded at an optimized flow rate (20 μl min^{-1}) and sampling interval (5 μs). Density plots were drawn to analyze the data distribution (Fig. 8). The dashed oval indicates the region designated to the electrical profiles of cancer cells determined from the pulse distribution shown in Fig. 7(a). The data showed that translocation profiles for more than 75% of cancer cells that spiked in mixed suspension were found in the defined area. This signified that our device could identify the cancerous cells with a detection efficiency of ~75%, an important metric

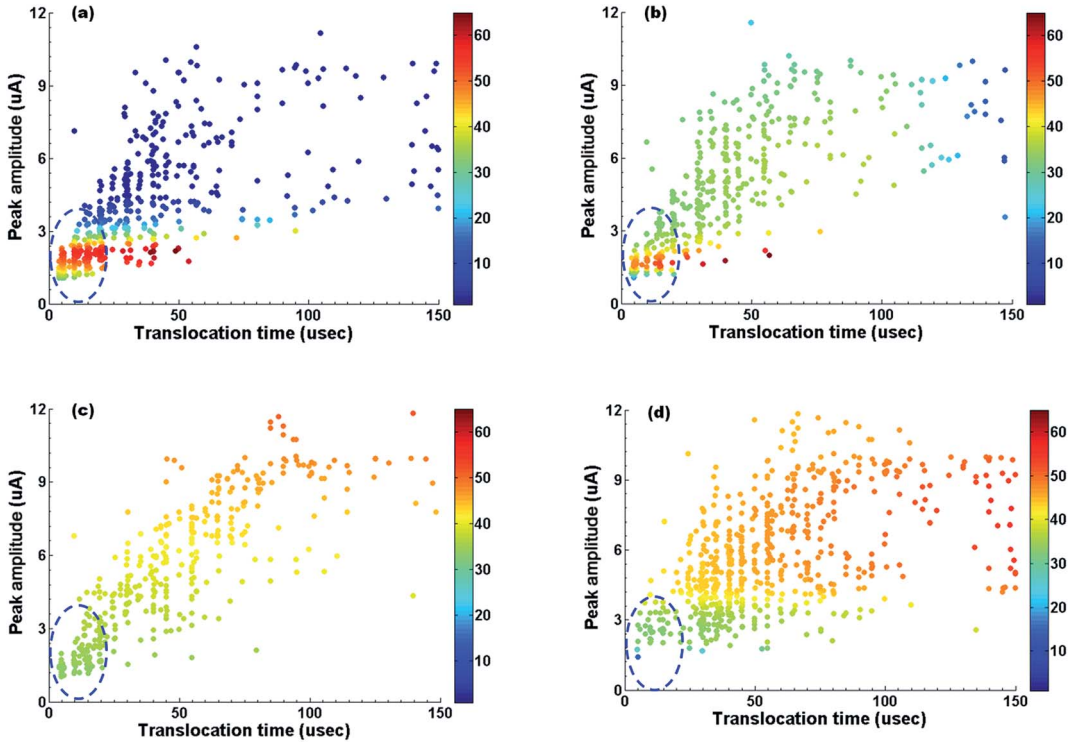

Fig. 8 Data density plots for cell suspensions mixed in different ratios. (a–d) show data density plots for cell suspension with the decreasing relative concentration of cancer cells: (a) 1 : 1, (b) 1 : 10, (c) 1 : 100 and (d) 1 : 1000. The cancer cells show distinctive current signals and can be efficiently identified out of a mixed-cell suspension as shown by the dashed ovals. The color map designates the relative data density distribution of the cells.

Table 1 Summary of pulse statistics for both cell types through a 20 μm micropore

	Cell types	
Measurement (units)	Bladder cancer cells	Normal urothelial cells
Average translocation time (μs)	8.48 ± 3.45	107 ± 89.06
Average peak amplitude (μA)	3.11 ± 1.04	5.64 ± 2.15

needed for biopsy samples. The device is thus capable of sensing abnormal cells even when there are only hundred cancer cells mixed with thousands of normal cells, which might be the possible cell population in a biopsy sample collected by FNA.

Although biopsy samples are very important sources for diagnosing cancer, conventional pathology faces high probabilities for false results and lacks statistical confidence. The presented approach has the potential to overcome many shortcomings by detecting cancer cells without relying on biomarkers, cell staining or experience. Moreover, the device is also capable of diagnosing cancer at earlier stages by screening each individual cell of biopsied sample, which is almost impossible in standard pathological testing. The recording of cell translocation pulses provides information about cell properties, and the analysis gives an affirmative determination of cancer cells. One order of magnitude difference in translocation time dictates the device's capability to undertake the highly intrinsic biomechanical properties of a cell as a robust discriminating factor for the early detection of cancer. The device can also be used for cell enumeration and phenotype characterization of investigated cells.

Conclusions

A novel approach to identify bladder cancer cells using solid-state micropores as the biological transducer is reported. Biophysical properties (cellular functions, physical dimensions, rigidity, growth rate, cytoskeleton) of cancer cells vary significantly from normal cells. PDMS microchannels also confirmed significant difference in the viscoelastic nature of bladder cancer cells and normal urothelial cells. The micropore device recorded the current blockage pulse for the translocated cell. The data discriminated the cancer cells from the statistical analysis based on the behavior of each cell in the investigated sample. High throughput, rapid detection, low cost, statistical validity, reliability, no need for cell staining and the utility of an inherent cell marker made this device a better alternative for early cancer diagnosis; moreover, it also offered a new window into other cellular processes that involve the mechanical properties of cytoskeleton.

Acknowledgements

We would like to thank M. R. Hasan for assistance with graphics and M. A. I. Mahmood for helpful remarks and discussions. The work was supported by a grant from the National Science Foundation (ECCS-1201878) to S. M. Iqbal. Azhar Ilyas acknowledges fellowship support from the Cancer Research Foundation of North Texas, Arlington, Texas, USA.

References

1 R. G. Sheiman, C. Fey, M. McNicholas and V. Raptopoulos, *Am. J. Roentgenol.*, 1998, **170**, 1603–1607.
2 V. Jeevanandam, M. R. Treat and K. A. Forde, *Gastrointest. Endosc.*, 1987, **33**, 370–371.
3 J. Melrose, S. Smith and P. Ghosh, in *Cartilage and Osteoarthritis*, Springer, 2004, pp. 39–63.
4 W. Bruening, J. Fontanarosa, K. Tipton, J. R. Treadwell, J. Launders and K. Schoelles, *Ann. Intern. Med.*, 2010, **152**, 238–246.
5 J. B. Haun, C. M. Castro, R. Wang, V. M. Peterson, B. S. Marinelli, H. Lee and R. Weissleder, *Sci. Transl. Med.*, 2011, **3**, 71ra16.
6 L. Y. Joanne and J. W. Rak, *Breast Cancer Res.*, 2003, **5**, 83–88.
7 E. L. Elson, *Annu. Rev. Biophys. Biophys. Chem.*, 1988, **17**, 397–430.
8 H. Lodish, A. Berk, S. L. Zipursky, P. Matsudaira, D. Baltimore and J. Darnell, *Molecular Cell Biology*, W. H. Freeman, New York, 1999.
9 P. Janmey, *Handbook of Biological Physics*, 1995, vol. 1, pp. 805–849.
10 K. Rao and H. J. Cohen, *Mutat. Res., DNAging: Genet. Instab. Aging*, 1991, **256**, 139–148.
11 A. Ben-Ze'ev, *Biochim. Biophys. Acta, Rev. Cancer*, 1985, **780**, 197–212.
12 H. Yamaguchi and J. Condeelis, *Biochim. Biophys. Acta, Mol. Cell Res.*, 2007, **1773**, 642–652.
13 M. Yilmaz and G. Christofori, *Cancer Metastasis Rev.*, 2009, **28**, 15–33.
14 J. Guck, S. Schinkinger, B. Lincoln, F. Wottawah, S. Ebert, M. Romeyke, D. Lenz, H. M. Erickson, R. Ananthakrishnan and D. Mitchell, *Biophys. J.*, 2005, **88**, 3689–3698.
15 M. Lekka, P. Laidler, D. Gil, J. Lekki, Z. Stachura and A. Z. Hrynkiewicz, *Eur. Biophys. J.*, 1999, **28**, 312–316.
16 K. A. Ward, W. I. Li, S. Zimmer and T. Davis, *Biorheology*, 1991, **28**, 301.
17 M. Radmacher, *Methods Cell Biol.*, 2002, **68**, 67–90.
18 J. Sleep, D. Wilson, R. Simmons and W. Gratzer, *Biophys. J.*, 1999, **77**, 3085–3095.
19 O. Thoumine and A. Ott, *Biorheology*, 1997, **34**, 309–326.
20 T. Kundu, J. Bereiter-Hahn and I. Karl, *Biophys. J.*, 2000, **78**, 2270–2279.
21 D. R. Gossett, T. K. Henry, S. A. Lee, Y. Ying, A. G. Lindgren, O. O. Yang, J. Rao, A. T. Clark and D. Di Carlo, *Proc. Natl. Acad. Sci. U. S. A.*, 2012, **109**, 7630–7635.
22 J. B. Wyckoff, J. G. Jones, J. S. Condeelis and J. E. Segall, *Cancer Res.*, 2000, **60**, 2504–2511.
23 A. ul Haque, M. Zuberi, R. E. Diaz-Rivera and D. Marshall Porterfield, *Biomed. Microdevices*, 2009, **11**, 1239–1250.
24 B. Matthews and J. W. Judy, *J. Microelectromech. Syst.*, 2006, **15**, 214–222.
25 M. Kitta, H. Tanaka and T. Kawai, *Biosens. Bioelectron.*, 2009, **25**, 931–934.
26 X. Niu and Z. Yan, *J. Biomed. Eng.*, 2001, **18**, 615.
27 H. Chang, A. Ikram, F. Kosari, G. Vasmatzis, A. Bhunia and R. Bashir, *J. Vac. Sci. Technol., B: Microelectron. Nanometer Struct.–Process., Meas., Phenom.*, 2002, **20**, 2058–2064.
28 W. Asghar, Y. Wan, A. Ilyas, R. Bachoo, Y. Kim and S. M. Iqbal, *Lab Chip*, 2012, **12**, 2345–2352.
29 W. Asghar, A. Ilyas, J. A. Billo and S. M. Iqbal, *Nanoscale Res. Lett.*, 2011, **6**, 1–6.
30 W. Asghar, A. Ilyas, R. R. Deshmukh, S. Sumitsawan, R. B. Timmons and S. M. Iqbal, *Nanotechnology*, 2011, **22**, 285304.
31 Y. Wan, D. Tamuly, P. B. Allen, Y.-t. Kim, R. Bachoo, A. D. Ellington and S. M. Iqbal, *Biomed. Microdevices*, 2012, 1–9.
32 J. B. Heng, A. Aksimentiev, C. Ho, P. Marks, Y. V. Grinkova, S. Sligar, K. Schulten and G. Timp, *Nano Lett.*, 2005, **5**, 1883–1888.
33 L. G. Collste, M. Devonec, Z. Darzynkiewicz, F. Traganos, T. K. Sharpless, W. F. Whitmore and M. R. Melamed, *Cancer*, 1980, **45**, 2389–2394.
34 T. Tansatit, S. Sahaphong, S. Riengrojpitak, V. Viyanant and P. Sobhon, *Vet. Parasitol.*, 2006, **135**, 269–278.
35 P. Chen, J. Gu, E. Brandin, Y. R. Kim, Q. Wang and D. Branton, *Nano Lett.*, 2004, **4**, 2293–2298.

